Sonar Performance Metrics Part 3

Marshall Bradley

This document illustrates how various types of uncertainty affect the forecasting of sonar performance in naval applications. The first type of uncertainty arises from the fact that we have incomplete knowledge regarding key target kinematic parameters such as range, bearing, depth, heading, speed, etc. In general key sonar performance metrics such as the sonar probability of detection P(D) are dependent upon each of these kinematic parameters. A second type of uncertainty is caused by the actual oceanographic environment in which the sonar operates. At a conceptual level, a sonar makes a mark on a gram or display when the voltage in a detector circuit exceeds a threshold. The probabilities with which these marks occur are determined by the statistics of the noise and signal that the sonar actually experiences. The statistical distribution of the signal and noise fields at the sonar receiver are strongly influenced by a nondeterministic component of ocean sound transmission. Numerous examples are presented.

Background

This document was originally written in 2010 when the author was a scholar in residence at Southeastern Louisiana University. It is presented here in a slightly updated format. In some instances the Mathematica code for computing the figures has been included. The original document contained an introduction and six sections. The section on entropy and sonar performance is presented here. The author is currently the Chief Scientist at LogLinear Group, LLC.

marshall.bradley@gmail.com
September 2022

5.0 Entropy and sonar performance prediction

5.1 Introduction

Consider the problem of an individual who must make a sonar performance prediction for a naval commander. We will initially suppose that the sonar is operated in an environment whose properties are completely known to the modeler. As we shall see this makes the modeler's job considerably easier. We will further suppose that the form of the signal radiated by the target is also known and that the sonar employs a matched filter detector. At this stage, the only uncertainty in the problem is the range r separating the target and the sonar. The naval commander would like to know how the performance of the sonar is influenced by range. To keep thing as simple as possible, we will assume that the acoustic propagation between the sonar and the target is just spherical spreading. Under these idealized circumstances the answer to the naval commander's question can be found by computing probabil

ity of detection for the sonar as a function of the range r separating the sonar and the target. We denote this quantity by $p_d(r)$ or $P(D \mid r)$. The symbol D denotes the event detection. Specifically in this case, the desired probability of detection can be expressed in terms of the cumulative probability density function $\Phi(y)$ of the Gaussian distribution:

$$p_d(r) = \Phi\left(\sqrt{2\, snr(r)} - z_{\text{pfa}}\right),$$

where

$$snr(r) = \frac{T\, p_0^2\, r_0^2}{N_0\, r^2},$$

and T is the signal integration time, p_0^2 is the target source level (on a power scale), r_0 is a reference distance (1 yd or 1 m), N_0 is the ambient noise spectral level (power/Hz) and z_{pfa} is a threshold parameter that is equal to 4.75342 for a receiver false alarm rate of 10^{-6}. If r is known, then p_d is determined with complete certainty. An example computation of $p_d(r)$ is shown in figure 5.1 for a 160 dB target source level, 80 dB ambient noise spectral level and a 1 sec integration time. With these choices of parameters

$$snr(r) = \frac{10^{(160-80)/10}}{r^2} = \frac{10^8}{r^2}.$$

As the range r increases, the signal to noise ratio $snr(r)$ rapidly decreases and the probability of detection quickly goes to zero. At ranges closer than 2000 yd, $p_d(r)$ is effectively 1. At ranges greater than 6000 yd, $p_d(r)$ is nearly zero. In between 2000 yd and 6000 yd, probability $p_d(r)$ rapidly decreases with the maximum rate of decrease occurring at a range of about 3000 yd.

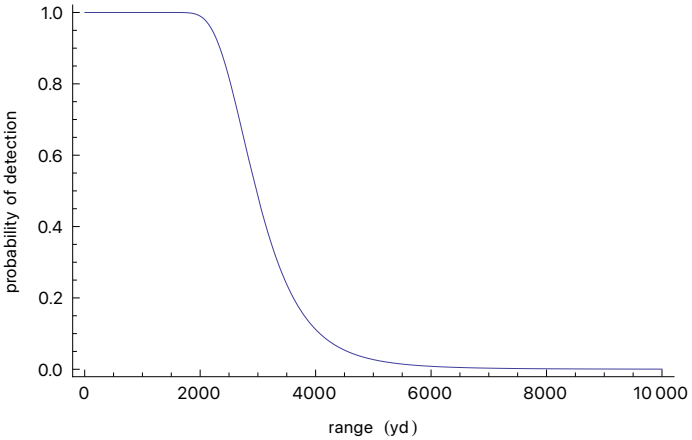

Figure 5.1. Probability of detection versus range in a $20\log_{10}(r)$ transmission loss environment with a match filter detector. The target source level is 160 dB and the ambient noise spectral level is 80 dB. The false alarm rate is 10^{-6}. The receiver integration time is 1 sec.

The simple scenario that we have posed in our discussion is obviously very unrealistic. No underwater acoustic modeler has complete knowledge of the ocean environment. The ocean surface is a dynamic, moving surface that can only be described stochastically. Internal waves and tidal effects modulate the water column and perturb the variation of sound speed with depth. The ocean bottom is rough

over a wide scale of wavelengths and the properties of the ocean bottom as they relate to the reflection, scattering and transmission of sound are imperfectly represented even in the best environmental data bases. The net result of these effects is that there is a degree of uncertainty associated with an acoustic model prediction and this uncertainty grows with increasing range, especially in circumstances where there are multiple interactions between the sound field and the ocean bottom and surface. The question now becomes how we should quantitatively address the effects of this uncertainty as it relates to performance prediction. The first step in answering this question is to define a performance metric that quantifies degree of uncertainty. We will describe the uncertainty in a performance prediction with a probability distribution. The amount of uncertainty in a probability distribution can be quantified via a concept known as entropy.

5.2 Entropy

A reasonable measure for the "amount of uncertainty" in a discrete probability distribution p_1, $p_{2,\ldots}$ p_n is the information entropy H (Jayne, 2003)

$$H(p_1, p_2, \ldots p_n) = -\sum_{i=1}^{n} p_i \log(p_i).$$

The concept of entropy in this context was originally developed by Claude Shannon (Shannon, 1948) in his pioneering studies on information theory. Information entropy is not related to the "entropy" of a thermodynamical process. Information entropy is a quantity that pertains strictly to probability distributions.

For discrete probability distributions, information entropy is maximal for the uniform distribution and minimal for a distribution in which all the probability is concentrated at a single point. As an example, suppose that we have two discrete probability distributions of length n. In the first distribution, the probabilities are all equal to $1/n$. In the second distribution, the probabilities are strongly concentrated at the first point. The probabilities at remaining $n - 1$ points in this second distribution are equal to a small number ϵ. The entropies of these two probability distributions are

$$H_1\left(\frac{1}{n}, \frac{1}{n}, \ldots \frac{1}{n}\right) = -n \frac{1}{n} \log\left(\frac{1}{n}\right) = \log(n),$$

$$H_2(1 - (n-1)\,\epsilon, \epsilon, \ldots \epsilon) = -\frac{1}{1 - (n-1)\,\epsilon} \log(1 - (n-1)\,\epsilon) - (n-1)\,\epsilon \log(\epsilon)$$

$\to 0$ as $\epsilon \to 0$.

Thus in this particular case, we see that the entropy is maximal for the uniform distribution $1/n$, $1/n$, ..., $1/n$ and minimal for the concentrated distribution 1, 0, …0.

For the case of the sonar performance prediction problem introduced in section 5.1, there was complete certainty in our knowledge of the environment. The probability density of the performance prediction is concentrated at a single point with probability 1. For example, at a range of 3000 yd, the probability of detection is 0.484 as shown in figure 5.1. Since there is no uncertainty associated with

our prediction process, the probability that we get this value is 1. The distribution of the prediction in probability space is

$P(p_d \mid r = 3000, C) = \delta(p_d - 0.484),$

where $\delta(p)$ denotes the Dirac delta function and C is used to denote the event of complete certainty in the environment. The entropy is

$H(1) = -1 \log(1) = 0.$

Now let us suppose that the transmission loss is not 20 log(r) but rather a range of three possibilities: 20 log(r) + 5 dB, 20 log(r), 20 log – 5 dB with corresponding probabilities 1/4, 1/2, 1/4. At a range of 3000 yd for a 160 dB target in 80 dB noise, the corresponding signal to noise ratio values are 5.46 dB, 10.46 dB, 15.46 dB and the probabilities of detection are 0.0178, 0.484, 1.000 as shown in figure 5.2. The distribution of the performance prediction in probability space is no longer concentrated at a single point but at three points. The distribution of the performance prediction in probability space is now

$$P(p_d \mid r = 3000) = \frac{1}{4}\,\delta(p_d - 0.178) + \frac{1}{2}\,\delta(p_d - 0.484) + \frac{1}{4}\,\delta(p_d - 1.00),$$

and the entropy is

$$H\left(\frac{1}{4}, \frac{1}{2}, \frac{1}{4}\right) = -\left[\frac{1}{4}\log\left(\frac{1}{4}\right) + \frac{1}{2}\log\left(\frac{1}{2}\right) + \frac{1}{4}\log\left(\frac{1}{4}\right)\right] = 1.040.$$

It is important to note that the entropy does not depend upon specific values of the probability of detection $p_d(r)$ but rather on the way in which the probability prediction is influenced by a priori uncertainty. It is also important to note that entropy is a measure of disorder, not spread.

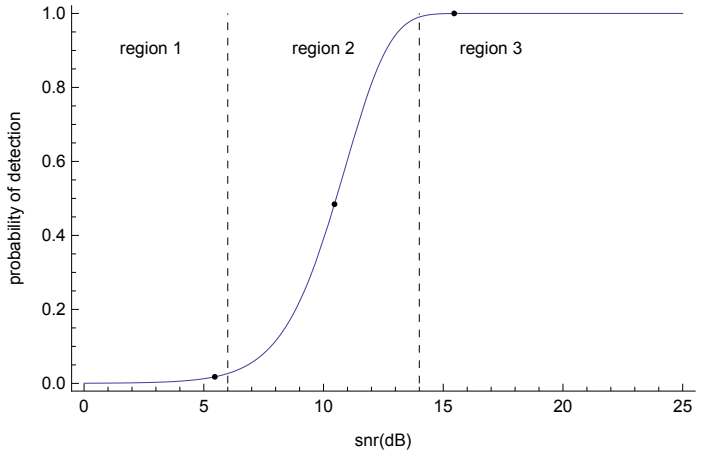

Figure 5.2. Performance of the matched filter as a function of signal to noise ratio. In region 1 p_d is nearly 0. In region 3 p_d is nearly 1. The transition from region 1 to 3 occurs over a *snr* range (region 2) that is 8-10 dB in width. The three points in the figure are p_d values at 5.46, 10.46 and 15.46 dB.

Returning to the example of the modeler and the naval commander, the situation has become much more complicated. The answer to the question, what is my performance at a range of 3000 yd, is no longer a single number. A truthful answer to the naval commander's question is the following: In 25 percent of the cases, the model indicates that the probability of detection is 0.178. In 50 percent of the

cases, the model indicates that the probability of detection is 0.484, and in the remaining 25 percent of the cases, the model indicates that probability of detection is 1.00. What should the modeler tell the naval commander? The mean probability of detection is

$$\overline{p}_d = \sum_{i=1}^{3} p_i\, p_d(i) = 0.484,$$

where p_i is 1/4, 1/2, 1/4 and $p_d(i)$ is 0.178, 0.484, 1.00. But using $\overline{p}_d = 0.484$ as an answer gives the naval commander no knowledge of the fact that this answer was only correct in half of the cases.

The naval commander needs to have some insight into the uncertainty in the information that is being provided. There are two types of uncertainty in the prediction. The first of these can be characterized by the entropy,

$$H(1/4,\ 1/2,\ 1/4) = 1.040,$$

which we have seen is a measure of the disorder in a distribution. The second type of uncertainty reflects the fact that there is scale-dependent spread in the distribution. This latter quantity can be characterized by the standard deviation,

$$\sigma(p_d) = \left[\sum_{i=1}^{3} p_i [p_d(i) - \overline{p}_d]^2\right]^{1/2} = 0.300.$$

An important distinction between these two quantities is that entropy only depends on the p_i values whereas the standard deviation depends on both the p_i values and the $p_d(i)$ values. Depending upon the application, one may be preferred over the other.

5.3 Uncertainty in transmission loss

In a realistic ocean environment it is not possible to predict the transmission $TL(r)$ with complete precision. As the range r separating the source and receiver increases, the effects of uncertainties in environmental knowledge become magnified. Multiple interactions of sound rays with the ocean surface and bottom make accurate predictions difficult. The net result is that we cannot characterize the transmission loss or more generally the signal to noise ratio by a single number at a given range. Transmission loss and the signal to noise ratio must be represented by a statistical distribution.

In order to quantify this problem, we will rely upon a detailed analysis of acoustic propagation predictions (Gough, 2001). In this analysis it was found that the uncertainty in transmission loss, or spread, increased with range. The statistical distribution of transmission loss in range was found to be governed by a Gumbel-type extreme value distribution. The probability density of transmission loss was found to be

$$P_{TL}(r) = \frac{e^{-e^{\frac{-(x-\alpha)}{\beta}} + \frac{-(x-\alpha)}{\beta}}}{\beta}$$

where $\alpha(r)$ is the modal transmission loss at range r in decibel units,

$$\alpha(r) = \begin{cases} 20 \log_{10}(r), & r < 1000 \\ 60 + 10 \log_{10}(r/1000) + 0.005\, r, & r \geq 1000 \end{cases},$$

and $\beta(r)$ is the spread in transmission loss

$$\beta(r) = 10 \log_{10}\left(\frac{r}{1000}\,\frac{\pi^2}{6}\right),$$

also measured in dB units. A plot of $P_{TL}(r)$ is shown in figure 5.3 for ranges of 1000 and 5000 yd. The transmission loss probability density is much more spread out at the longer range. For reference, transmission loss with spherical spreading and Rayleigh uncertainty (5.57 dB) is also shown in figure 5.3.

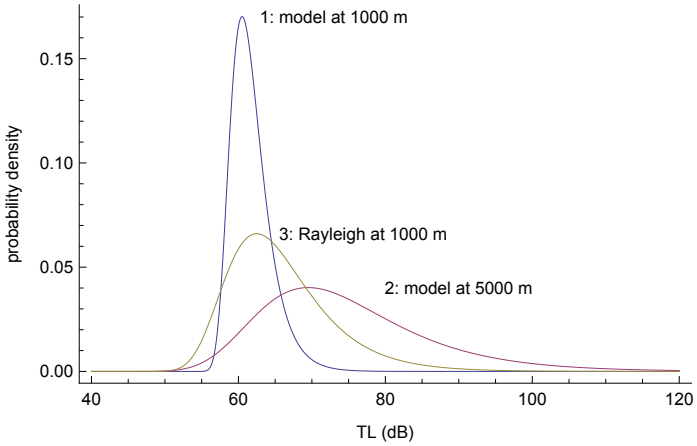

Figure 5.3. Probability density of transmission loss at 1000 yd and 5000 yd with spherical spreading with Rayleigh fluctuations reference curve.

5.4 The effect of transmission loss uncertainty on the distribution of probability of detection

The uncertainty in transmission loss depicted in figure 5.3 causes uncertainty in the signal-to-noise ratio, which in turn leads to uncertainty in the prediction of a probability of detection. Ideally for a given range r, we would like to be able to analytically calculate the probability distribution $P(p_d \mid r)$ that is caused by the environmental uncertainty as characterized by the transmission probability distribution $P_{TL}(r)$ and other sources of uncertainty. In all but the simplest of cases, this cannot be done analytically and we must resort to numerical techniques. We have done this via a Monte Carlo technique. For a given range, we generate 10000 realizations of TL values from the distribution $P_{TL}(r)$. These TL values are then used, with the aid of the sonar equation, to compute a corresponding set of p_d values. Then we calculate a relative histogram from the 10000 p_d values. This relative histogram is used as an estimate of the probability distribution of the performance prediction $P(p_d \mid r)$. Examples of this are shown in figures 5.4-5.8 for ranges of 1000, 2000, 3000, 5000 and 10000 yd. The variation of the entropy of $P(p_d \mid r)$ with range is shown in figure 5.9 and the variation of the standard deviation of $P(p_d \mid r)$ with range is shown in figure 5.10.

The range in figure 5.4 is 1000 yd and signal-to-noise ratio values are high. The sonar is operating in region 3 of figure 5.2 and the probability of detection is tightly concentrated near $p_d = 1$. The entropy and standard deviation of the probability distribution $P(p_d \mid r = 1000)$ are respectively 1.09 and 0.106. In figure 5.5 the range is 2000 yd and the probability distribution $P(p_d \mid r = 2000)$ has become bifurcated with peaks in probability density near probability values of 0 and 1. The peak near 0 is more pronounced. The entropy and standard deviation are now respectively 2.60 and 0.400, and the mean is no longer a good measure of central tendency. In figure 5.6, the range is 3000 yd and the probability distribution $P(p_d \mid r = 3000)$ is completely bifurcated with entropy and standard deviation values of 2.68 and 0.444. In figure 5.7 the range is 5000 yd. The probability distribution $P(p_d \mid r = 5000)$ is still bifurcated but the probability of detection is now more concentrated near 0. The entropy and standard deviation are 2.34 and 0.436. At 10000 yd as shown in figure 5.8, the probability of detection has become more concentrated near probability values of 0 but there is still a strong second peak near the probability value 1. The entropy and standard deviation have decreased to 1.69 and 0.369.

The variation of entropy with range is shown in figure 5.9. A similar result for the standard deviation is shown in figure 5.10. Maximum entropy occurs at a range of about 2500 yd and the maximum standard deviation occurs at a range of about 3000 yd.

The unusual behavior of the probability distributions shown in figures 5.4- 5.8 can be explained with the aid of figure 5.11. This figure shows a plot of probability of detection as a function of signal-to-noise ratio (*SNR*) for the matched filter at a false alarm rate of 10^(-6). The probability density curves have been normalized so that they fit on the same scale as $p_d(SNR)$. At a range of 1000 yd, the probability density of SNR is almost entirely in the range where the matched filter has a probability of detection equal to unity. At 2000 yd, the probability density of SNR is more evenly spread over the range where the probability of detection $p_d(SNR)$ quickly changes from near zero to unity. At ranges of 5000 yd and 10000 yd, the probability density of SNR is spread out over a much wider range and overlaps with both tails of the function $p_d(SNR)$.

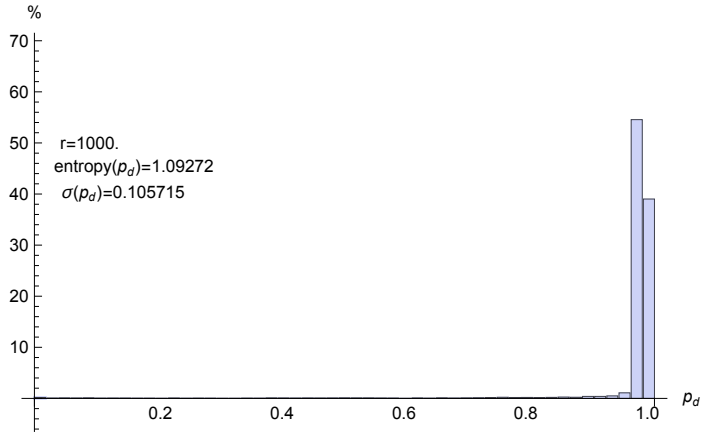

Figure 5.4. Probability density of the performance $P(p_d \mid r)$ at r=1000 yd.

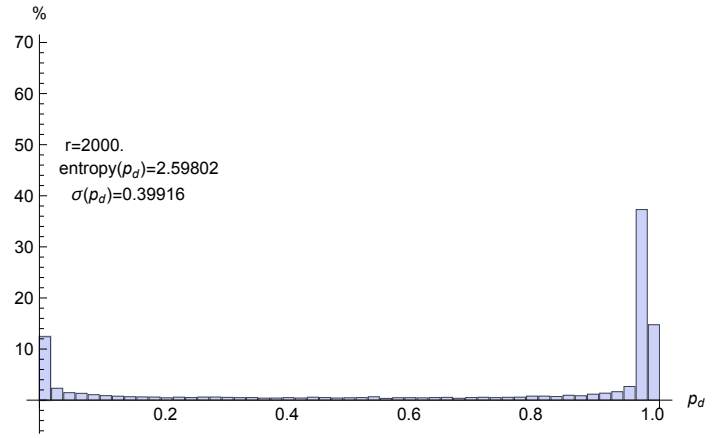

Figure 5.5. Probability density of the performance $P(p_d \mid r)$ at r=2000 yd.

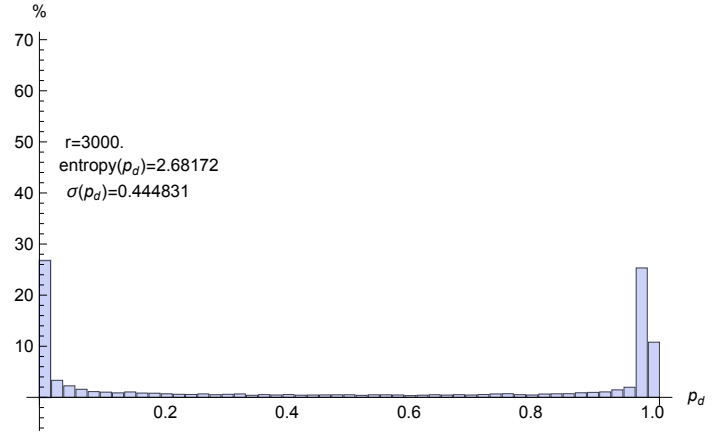

Figure 5.6. Probability density of the performance $P(p_d \mid r)$ at r=3000 yd.

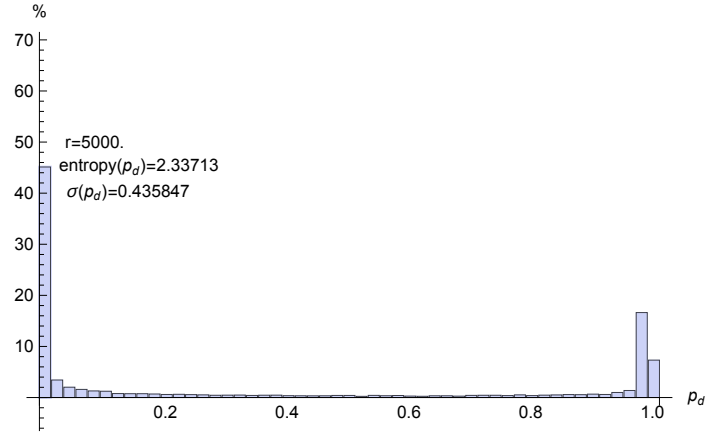

Figure 5.7. Probability density of the performance $P(p_d \mid r)$ at r=5000 yd.

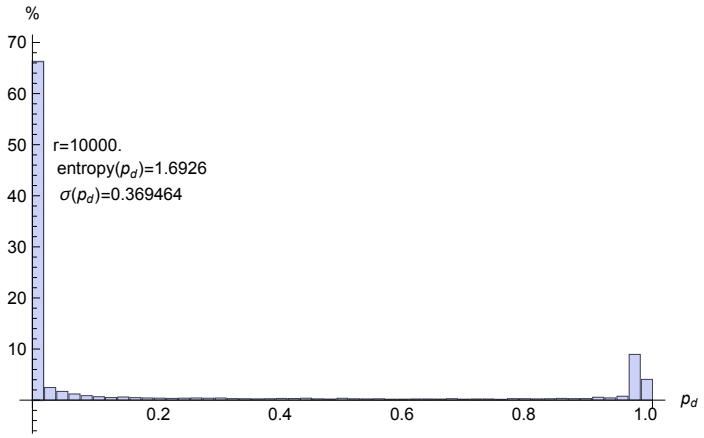

Figure 5.8. Probability density of the performance $P(p_d \mid r)$ at r=10000 yd.

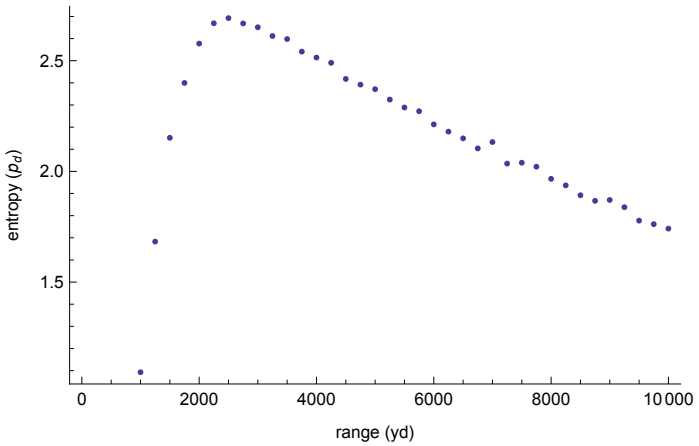

Figure 5.9 Entropy of probability density of the performance $P(p_d \mid r)$.

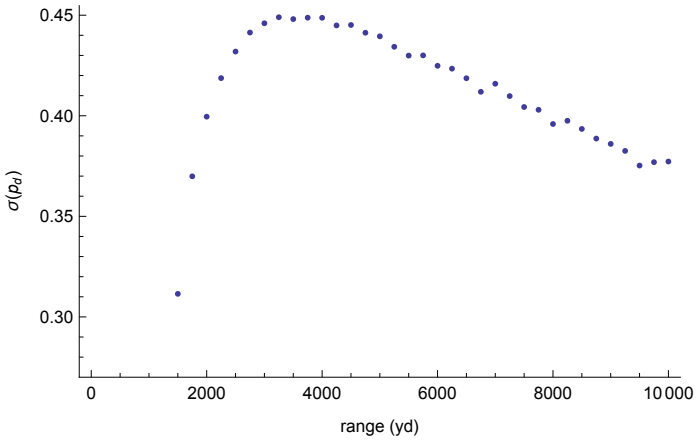

Figure 5.10. Standard deviation of probability density of the performance $P(p_d \mid r)$.

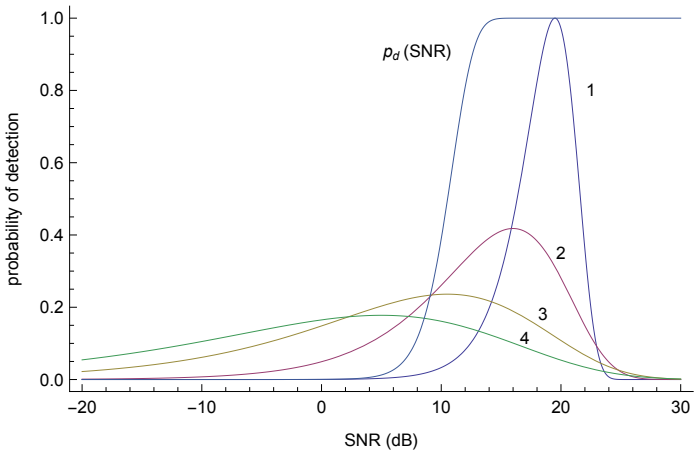

Figure 5.11. Probability of detection as a function of SNR for the matched filter false alarm rate of 10^(-6). Also shown are are the probability densities are range s of 1) 1000 yd, 2) 2000 yd, 3) 5000 yd and 4) 10000 yd. The source level is 160 dB and the noise level is 80 dB.

5.5 Range weighting to reduce false contacts

Consider a scenario in which an active sonar is operating in region with two types of targets. The first type of target is fish and the second type of target is enemy submarines. The fish are much more numerous than enemy submarines, but they have a much lower target strength thereby making them more difficult to detect at long ranges. As a result of their lower target strength, fish can only be detected at relative short ranges. Figure 5.12 shows the lateral range curves for fish (target type 1) and submarines (target type 2). The target strength (*TS*) of the fish and submarine are respectively assumed to be -5 and 10 dB. The sonar source level is 220 dB. The sonar is being operated in an environment with an 80 dB masking level. A matched filter receiver has been assumed with a false alarm rate of 10^(-6).

Suppose that a detection occurs at a particular range r. A question of great practical significance is the following: What is the probability that this detection at range r is caused by an echo from a fish. In order to address this question we proceed in the following fashion. Let H_1 denote the hypothesis that the echo is caused by a fish and H_2 denote the hypothesis that the echo is caused by an enemy submarine. If we let $P(H_1 \mid r)$ and $P(H_2 \mid r)$ denote the probability of hypotheses 1 and 2 given the event detection at range r, then Bayes theorem tells us that

$$P(H_1 \mid r) = \frac{P_d(r \mid H_1)\, P(H_1)}{P_d(r \mid H_1)\, P(H_1) + P_d(r \mid H_2)\, P(H_2)}$$

$$P(H_2 \mid r) = \frac{P_d(r \mid H_2)\, P(H_2)}{P_d(r \mid H_1)\, P(H_1) + P_d(r \mid H_2)\, P(H_2)},$$

where $P(H_1)$ and $P(H_2)$ denote the probabilities of hypothesis 1 and 2 and $P_d(r \mid H_1)$ and $P_d(r \mid H_2)$ denote the sonar's detection capability against type 1 and 2 targets as shown in figure 5.12. The probabilities $P(H_1)$ and $P(H_2)$ are known as the a priori probabilities of hypotheses 1 and 2 and their values are based upon the relative concentrations of type 1 and type 2 targets.

The Bayes probabilities $P(H_1 \mid r)$ and $P(H_2 \mid r)$ are shown in figure 5.13 for the case $P(H_1) = 0.999$ and $P(H_2) = 1 - P(H_2)$ are shown in figure 5.13. The lateral range curve for the type 2 target (submarine) is also shown in the figure for reference. Out to about a range of 1500 yd, if a contact occurs the probability is nearly unity that it comes from a fish. Beyond 1500 yd, sonar performance against fish becomes poor and $P(H_1 \mid r)$ decreases and reaches a minimum at 3000 yd. At ranges beyond 3000 yd, sonar performance against submarines becomes poor and $P(H_1 \mid r)$ increases. At longer ranges where the sonar works poorly against both target types, Bayes theorem simply tells us that contacts (if they occur) come from the most prevalent type of target (fish). The Bayes probability $P(H_2 \mid r)$ is directly related to $P(H_1 \mid r)$ via $P(H_2 \mid r) = 1 - P(H_1 \mid r)$. The shape of the plot of $P(H_2 \mid r)$ clearly lends itself to the concept of false target reduction.

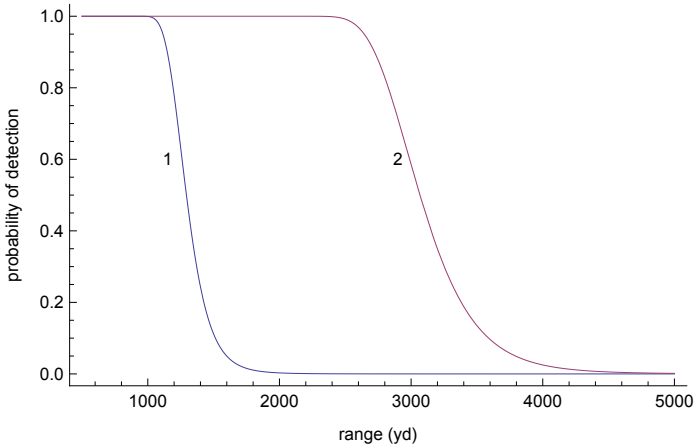

Figure 5.12. Lateral range curves $P_d(r \mid H_1)$ and $P_d(r \mid H_2)$ for fish (type 1 target) and submarines (type 2 target).

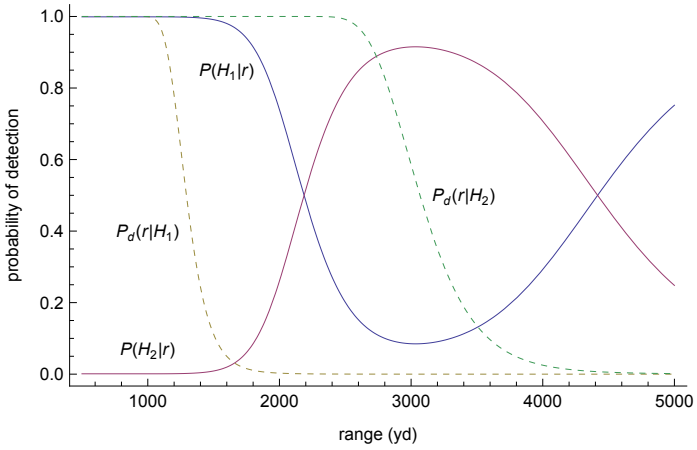

Figure 5.13. The Bayes probabilities $P(H_1 \mid r)$ and $P(H_2 \mid r)$ for fish (type 1 target) and submarines (type 2 target).

5.6 Probability of detection confidence interval

Consider a scenario in which the uncertainty in a performance prediction arises from the uncertainties inherent in the computation of transmission loss. In this case a confidence interval for probability of

detection can be found using the following technique. First compute a confidence interval for the transmission loss and then compute the probability of detection using the endpoints of the transmission loss confidence interval. Following (Gregory, 2005), we say an allowed range for transmission loss at a range r with probability content C (e.g., C=0.90 or 90%) is provided by a credible region defined by

$$\int_{TL_1}^{TL_2} p(TL \mid r)\, dTL = C,$$

where the transmission loss probability density $p(TL \mid r)$ within the interval (TL_1, TL_2) is everywhere greater than outside the interval. An example of this is shown in figure 5.14 at r = 1200 yd. A 90% confidence interval for the transmission loss extends from 57.3 to 68.7 dB. The confidence interval includes the modal TL value at 1200 yd. For a source level of 160 dB and an 80 dB ambient noise spectral level, these TL values correspond to a signal-to-noise (SNR) range of 11.3 to 22.7 dB. For a matched filter detector operating at a false alarm rate of 10^(-6), these SNR values in turn correspond to a probability of detection range 0.667 to 1.00. Thus

$$(p_{d1}, p_{d2}) = (0.667, 1.00),$$

can be viewed as 90% confidence interval for probability of detection. At ranges beyond 2000 yd as shown in figure 5.15, the 90% confidence interval for probability of detection is very nearly (0,1). This indicates that the uncertainties in transmission loss (and as a result in SNR) make it impossible to reliability predict the probability of detection.

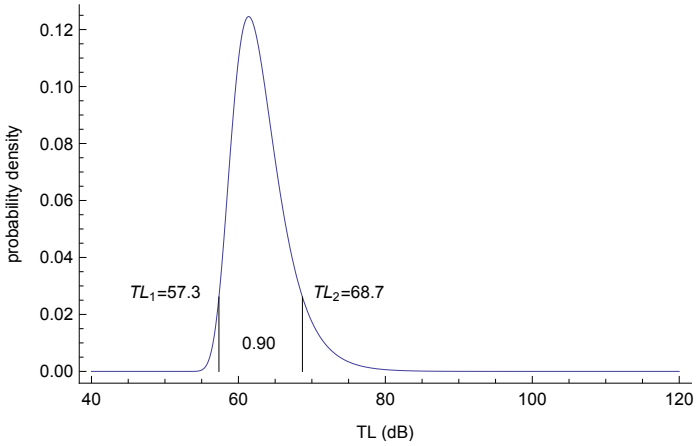

Figure 5.14. Confidence interval (90%) for transmission loss at 1200 yd.

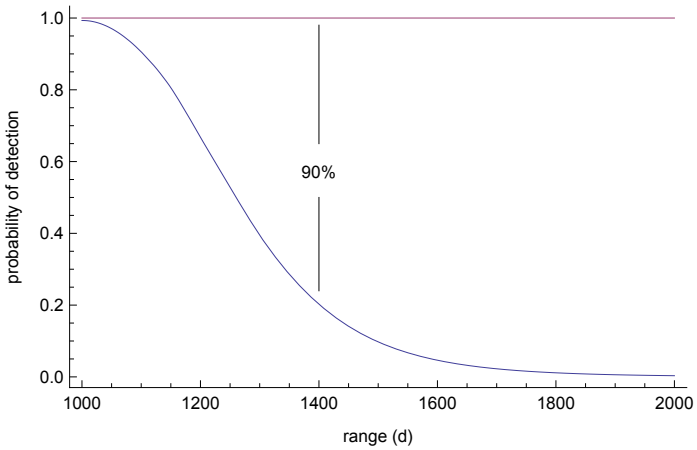

Figure 5.15. Upper and lower limits for a 90% confidence interval for probability of detection.

5.7 Analytic distribution of probability of detection with entropy computations

In a situation where there is uncertainty associated with a prediction of the signal-to-noise ratio (*snr)* that is to be used to compute the probability of detection (p_d) for a sonar system, it is very informative to investigate the behavior of the distribution of probability of detection that results from the *snr* uncertainty. To this end we consider the following canonical problem. Suppose that X is a random variable with probability density function $f(x)$ defined on the interval $x_1 < x < x_2$. Let $Y = u(X)$ denote a continuous increasing function of X with inverse function $X = v(Y)$. In terms of our application we can think of X as being the signal-to-noise ratio (*snr*) at the input to a sonar detector. The function $u(X)$ represents the mapping from *snr* space to probability of detection space. Since X is a random variable, Y is a random variable also. We are interested in determining the probability density function $g(y)$ of the random variable Y. By definition the cumulative distribution function of Y is

$$G(y) = P(Y < y) = P[u(X) < y] = P[X < v(y)]$$
$$= \int_{x_1}^{v(y)} f(x)\, dx.$$

Differentiation of $G(y)$ leads to

$$g(y) = f[v(y)]\, v'(y),\ u(x_1) < y < u(x_2)$$
$$= 0,\ \text{otherwise.}$$

As an example of this technique for computing the probability density function of the transformation of a random variable, suppose that X is exponentially distributed and that $Y = \sqrt{X}$. Then the probability density function of X is

$$f(x) = \frac{1}{\theta} e^{-x/\theta},\ 0 < x < \infty,$$

The probability density function $g(y)$ is

$$g(y) = f[v(y)]\, v'(y) = \frac{1}{\theta} 2y\, e^{-y^2/\theta},\ 0 < y < \infty,$$

which is the probability density function of a Rayleigh distributed random variable . In the foregoing we used $dv/\mathrm{dy} = 2y$.

In order to apply this analytical technique for computing the probability density function $g(y)$ to sonar detection problems, the mapping $u(x)$ from *snr* space to probability of detection space must be invertible in closed form. In most cases this is not true. There is however one important signal detection model that leads to an invertible mapping. Whalen (1971) treated the case of a signal with random phase and amplitude. The frequency and arrival time of the signal were assumed to be known to the receiver. However, the phase of the signal was assumed to be uniformly distributed on the interval $(0, 2\pi)$ and the amplitude A of the signal was assumed to be Rayleigh distributed with probability density function

$$w(A) = \frac{A}{A_0^2} \exp\left[-\frac{A^2}{2A_0^2}\right],\ 0 < A < \infty.$$

Whalen notes that this is a case of slow Rayleigh fading and that it is similar to the problem of detecting a Gaussian signal in Gaussian noise. The optimal receiver for detecting a signal with random phase and Rayleigh amplitude is a matched filter followed by an envelope detector. Whalen shows that the probability of detection as a function of signal-to-noise ratio E_{av}/N_0 and false alarm rate p_{fa} is

$$p_d(snr, p_{\mathrm{fa}}) = (p_{\mathrm{fa}})^{\frac{1}{1+snr}},$$

$$snr = A_0^2\, T/N_0 = E_{\mathrm{av}}/N_0,$$

where T is the time interval over which the signal is observed and N_0 is the background white noise spectral density. The quantity *snr* is the signal-to-noise ratio measured on an intensity (or power) scale.

A computation of $p_d(snr, p_{\mathrm{fa}})$ is shown in the accompanying figure for a false alarm rate of 10^(-6). At large values of the signal-to-noise ratio *snr,* amplitude fading and uncertainties in phase cause a significant degradation in receiver performance in comparison with the matched filter (all signal parameters known). At low signal-to-noise ratio the opposite is true.

We will determine the distribution of probability of detection for the case in which the signal-to-noise ratio *snr* is uniformly distributed in intensity space. We will denote *snr* by the variable x and assume that the probability density function $f(x)$ is

$$f(x) = \frac{1}{x_2 - x_1},\ x_1 < x < x_2,$$

0, otherwise,

where $x_1 = snr_0/\alpha$ and $x_2 = \alpha \cdot snr_0$. The interval (x_1, x_2) when converted to a decibel scale is $(SNR_0 - 10\log\alpha, SNR_0 + 10\log\alpha)$. We will use values of the parameter α equal to $\sqrt{2}$, 2 and 4, corresponding to decibel (dB) widths of ±1.5, ±3 and ±6 dB in the distribution of signal-to-noise ratio. The mapping from probability of detection space to signal-to-noise ratio space and its derivative are

$$v(p_d) = \frac{\log(p_{\mathrm{fa}})}{\log(p_d)} - 1,$$

$$v'(p_d) = -\frac{\log(p_{\text{fa}})}{p_d \log(p_d)^2}$$

The probability density function $g(p_d)$ of probability of detection is

$$g(p_d) = f[v(p_d)]\, v'(p_d) = -\frac{1}{\alpha \cdot snr_0 - snr_0/\alpha}\, \frac{\log(p_{\text{fa}})}{p_d \log(p_d)^2},\ p_{\text{d1}} < p_d < p_{\text{d2}}$$

$$0,\ \text{otherwise},$$

where $p_{\text{d1}} = p_d(snr_0/\alpha,\, p_{\text{fa}})$ and $p_{\text{d2}} = p_d(\alpha \cdot snr_0,\, p_{\text{fa}})$.

Computations of the probability density function $g(p_d)$ of probability of detection for values of snr_0 equal to 3, 10, 17 and 26 dB are shown in figures 5.17, 5.18 and 5.19. In figure 5.17 the uncertainty in signal-to-noise ratio is small (±1.5 dB). When the *snr* is small (3 dB), the probability density is tightly concentrated near $p_d = 0$. When the *snr* is large (26 dB), the probability density is tightly concentrated near $p_d = 1$. At intermediate values of the *snr* (10 and 17 dB), the probability density is more spread out. Figures 5.18 and 5.19 show that as the uncertainty or spread in *snr* increases to ±3 dB and ±6 dB, the spread in probability of detection becomes much larger.

At this point it is desirable to characterize quantitatively the amount of uncertainty in the probability density function $g(p_d)$. The appropriate measure of the uncertainty associated with a continuous probability density function $p(y)$ is the entropy:

$$S = -\int p(y) \log\left[\frac{p(y)}{m(y)}\right] dy,$$

where the $m(y)$ is called the Lebesgue measure and is chosen to ensure that the entropy is invariant under a change of variables (Gregory 2005). For our purposes we can assume that $m(y)$ is unity and simply compute the entropy via

$$S = -\int_{p_{\text{d1}}}^{p_{\text{d2}}} g(p_d) \log[g(p_d)]\, dp_d.$$

Figure 5.20 shows the entropy computation for uniformly distributed signal-to-noise ratio at three levels of uncertainty. When the uncertainty in the *snr* probability distribution is small (±1.5 dB), entropy levels are relatively small with a broad peak near about 12 dB. As the uncertainty in *snr* increases to ±3 dB and ±6 dB, the entropy becomes much more negative reflecting increased spread in the underlying probability distribution of probability and overall loss of information content. Minimum entropy occurs for *snr* values in the region of rapid increase in probability of detection for the signal detection model. In figure 5.21 the entropy computation is shown in a 3-D format. Figures 5.20 and 5.21 together with figures 5.17-5.19 imply that a prediction of probability of detection that has a very large, negative level of entropy associated with it is of little practical value due to the wide spreads in p_d associated with large, negative values of entropy.

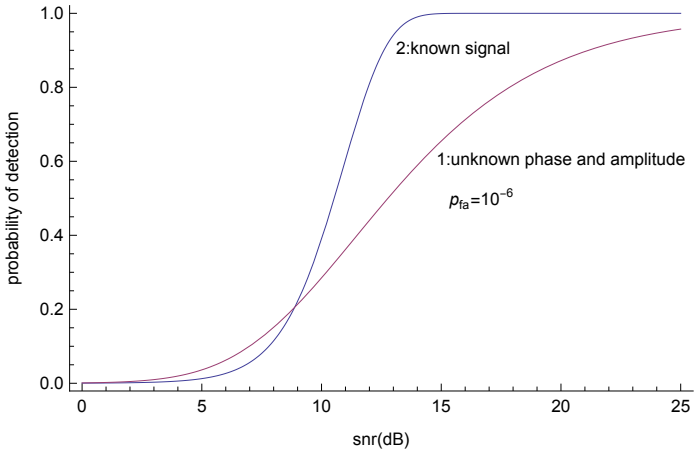

Figure 5.16. Detection performance of a Rayleigh fading signal (1) and a signal with known amplitude and phase (2).

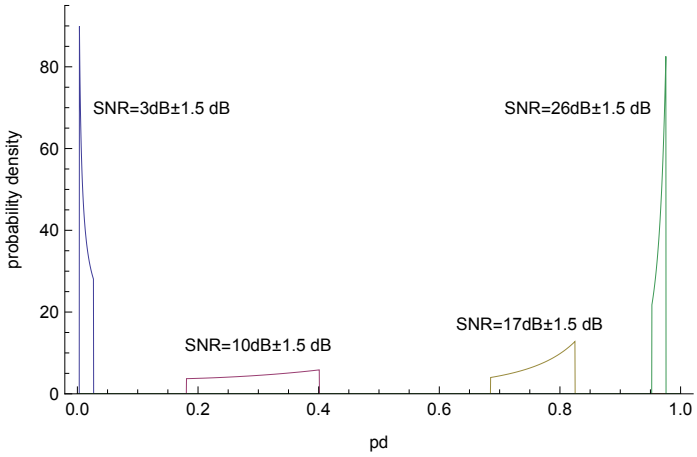

Figure 5.17. Probability density of probability of detection for uniformly distributed signal-to-noise ratio uncertainty with ±1.5 dB width.

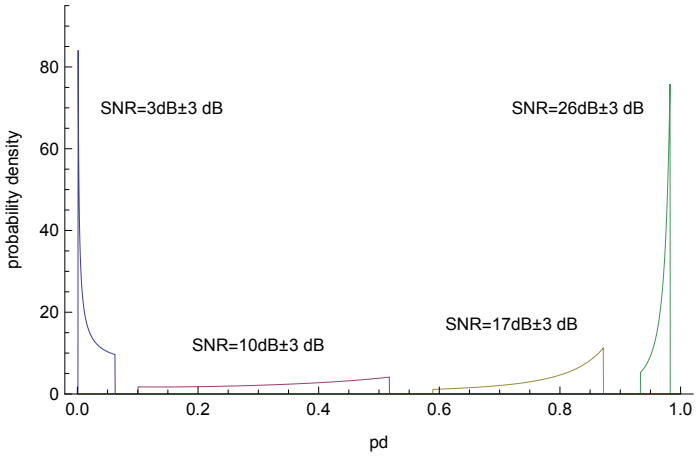

Figure 5.18. Probability density of probability of detection for uniformly distributed signal-to-noise ratio uncertainty with ±3 dB width.

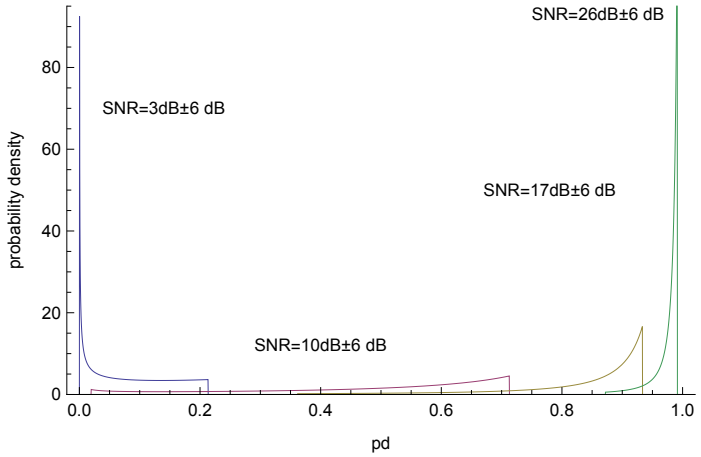

Figure 5.19. Probability density of probability of detection for uniformly distributed signal-to-noise ratio uncertainty with ±6 dB width.

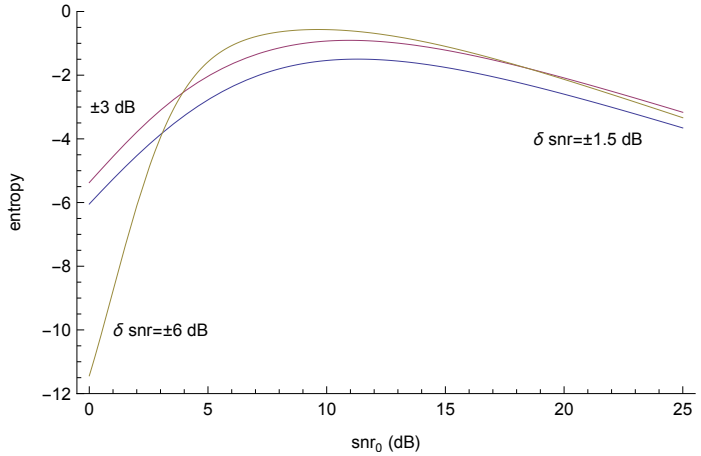

Figure 5.20. Entropy of probability density of probability of detection for three levels of uncertainty in *snr*.

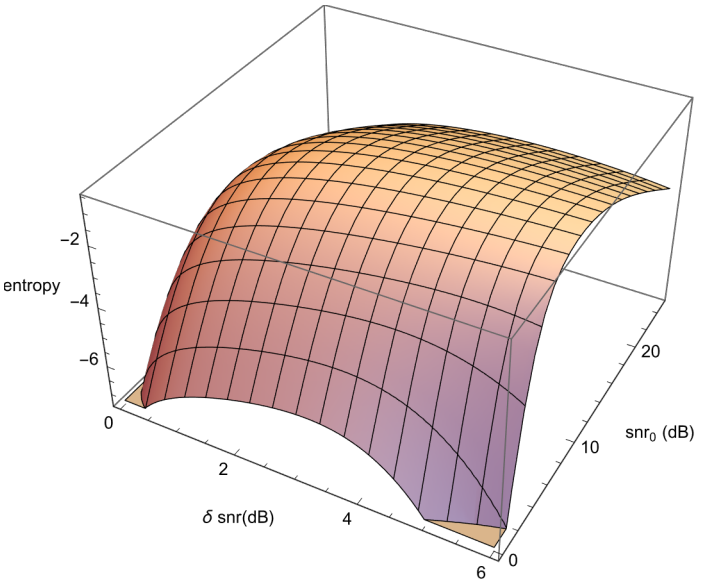

Figure 5.21. Entropy of probability density of probability of detection for uniformly distributed signal-to-noise ratio.

5.8 Probability distribution of average decay law transmission loss

Brekhovskikh and Lysanov (1982) develop a simple model for computing transmission that has been range-averaged over ray cycle distances. This model was originally developed by Smith (1974). The operation ⟨⟩ within the model represents averaging over the cycle distance of a ray. According to the model, the range-averaged, squared acoustic pressure at horizontal distance r from a reference source in a waveguide of depth h is

$$\langle \mid p \mid^2 \rangle = \frac{4}{r} \int_0^{\pi/2} \mid V(\chi_h) \mid^{2N} \exp(-\beta r) \frac{\cos(\chi_1)}{D(\chi_1) \sin(\chi)} d\chi_1,$$

where χ, χ_1 and χ_h respectively denote the grazing angle of a sound ray at the depth of the receiver, source and ocean bottom. The quantity $D(\chi_1)$ is the cycle distance of a ray that emanates from the source at angle χ_1, $V(\chi_h)$ is the amplitude reflection coefficient at the ocean bottom, and $N = N(\chi_h)$ is the number of bottom reflections that a ray makes in propagating out to horizontal distance r. To a reasonable degree of approximation $N \approx r / D(\chi_h)$. The angles χ, χ_1 and χ_h are related by Snell's law:

$$\frac{\cos(\chi)}{c} = \frac{\cos(\chi_1)}{c_1} = \frac{\cos(\chi_h)}{c_h},$$

where c, c_1 and c_h are the sound velocities at the depth of the receiver, source and ocean bottom.

If the waveguide is isovelocity ($c = c_1 = c_h$), then the ray cycle distance is simply

$$D(\chi_1) = 2\, h \cot(\chi_1),$$

and the range averaged squared acoustic pressure can be written in the form

$$\langle \mid p \mid^2 \rangle = \frac{\pi}{r\, h} \exp(-\beta r) \frac{2}{\pi} \int_0^{\pi/2} \mid V(\chi) \mid^{\frac{r}{h} \tan(\chi)} d\chi.$$

The leading factor in this expression

$$\frac{\pi}{r\, h} \exp(-\beta r)$$

simply represents cylindrical spreading with attenuation and the second factor

$$\frac{2}{\pi} \int_0^{\pi/2} \mid V(\chi) \mid^{\frac{r}{h} \tan(\chi)} d\chi$$

describes the amount of acoustic energy that is absorbed into the bottom.

We will first consider the case of a downward refracting waveguide with linear decrease in sound velocity from the ocean surface to the bottom and we will further suppose that our source is located near the surface and that the receiver is located midway between the surface and the bottom. In this type of environment the ray paths are arcs of circles and the ray cycle distance can be shown to be

$$D(\chi_1) = 2\, h \cot[(\chi_1 + \chi_h)/2],$$

where h denotes the water depth. In order to simplify computations we will assume that the bottom reflection loss coefficient $V(\chi_h)$ is independent of the bottom grazing angle χ_h. By choosing the sound-

speed at the ocean bottom to be just slightly less than the soundspeed at the ocean surface, we can also model sound propagation in an isovelocity waveguide with this model.

Computations of transmission loss in a downward refracting environment with surface soundspeed of 1500 m/s and bottom sound speed of 1480 m/s are shown in figure 5.22. The acoustic source is assumed to be located near the surface. The water depth is 300 m and the receiver is located at the midpoint of the water column. Three levels of bottom loss are considered: 1.5 dB, 3 dB and 6 dB. Figure 5.23 shows similar computations in an isovelocity environment. In both environments all ray paths interact with the bottom. However, ray cycle distances are shorter in the downward refracting environment. This results in more bottom interactions per distance traveled and higher overall transmission losses.

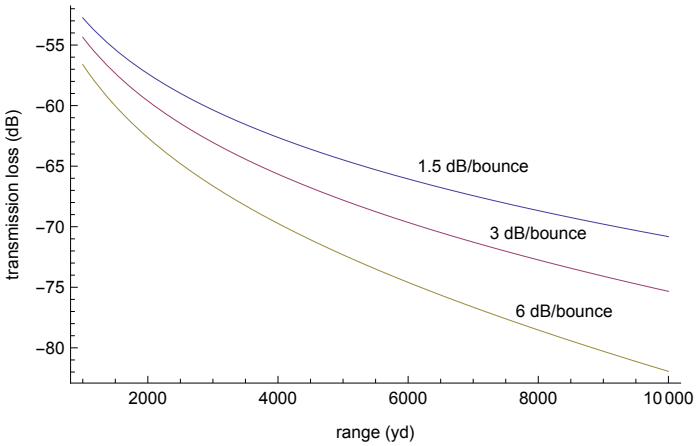

Figure 5.22. Range averaged transmission loss in a downward refracting environment.

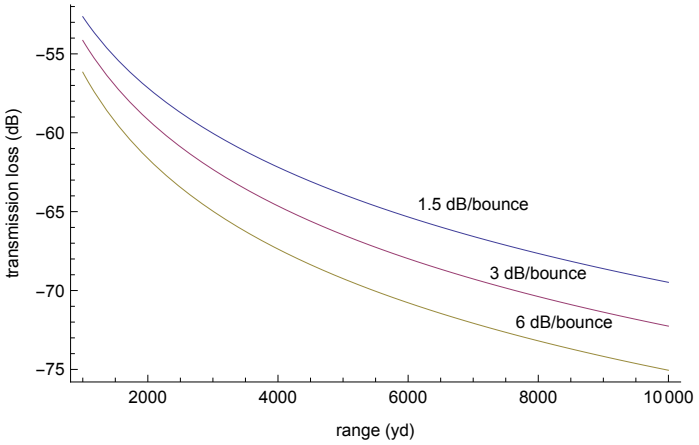

Figure 5.23. Range averaged transmission loss in an isovelocity environment.

In a realistic situation, the properties of the ocean bottom are not known with great certainty. This means that in a bottom interacting environment, the uncertainty associated with a transmission loss prediction will grow with range. In order to obtain some feel for the size and significance of this phenomena, we will model the ocean bottom reflectivity via an extreme value distribution with parameters $\alpha = 3$ dB and $\beta = 1$ dB . The probability density function of this bottom loss model is shown in figure 5.24. The modal bottom loss value is $\alpha = 3$ dB.

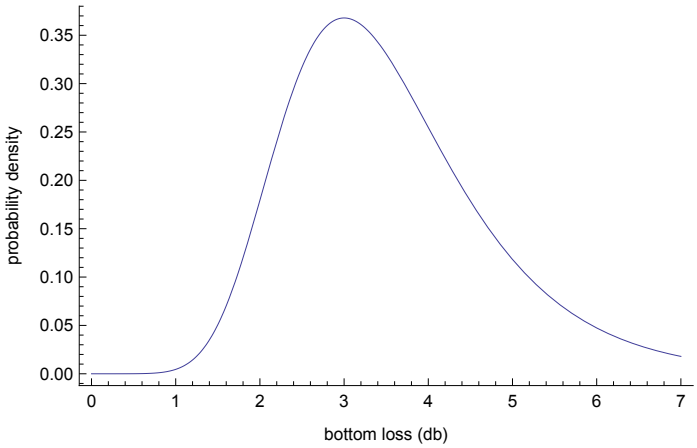

Figure 5.24. Probability distribution of bottom loss used in simulations.

We would like to calculate the distribution of transmission loss at different ranges. Even simple transmission loss models like the one considered in this section do not lend themselves to analytic calculations. To this end we compute the transmission loss distributions using a Monte Carlo approach. Figures 5.25 and 5.26 show probability density histograms for transmission loss at ranges of 1000 yd, 3000 yd and 10000 yd. Simulations were also performed at 20000 yd. At each range 10000 Monte Carlo realizations of transmission loss (TL) were computed based upon the bottom loss model depicted in figure 5.24. Figure 5.25 shows the results for the downward refracting environment and figure 5.26 shows the results for the isovelocity environment. Mean TL, standard deviation of TL and skewness of TL for the downward refracting environment and the isovelocity environment are tabulated in table 5.1 and 5.2.

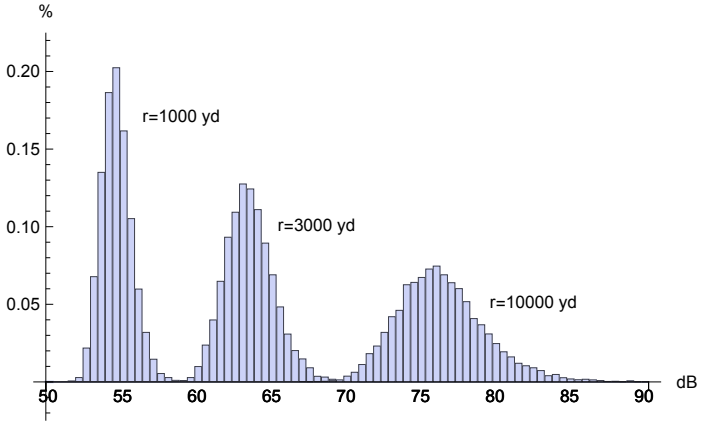

Figure 5.25. Probability distribution of transmission loss in a downward refracting environment.

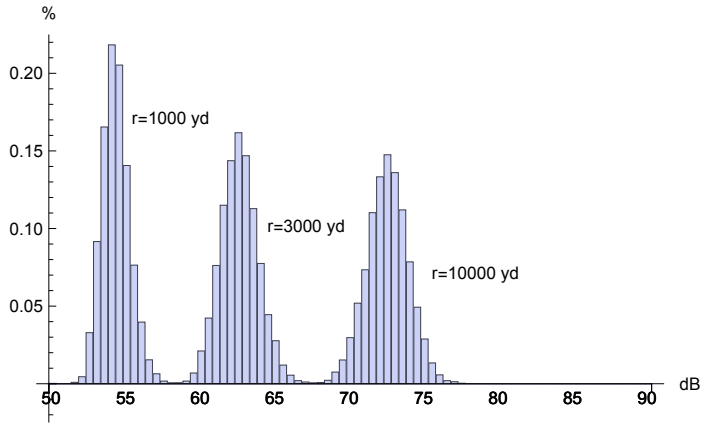

Figure 5.26. Probability distribution of transmission loss in an isovelocity environment.

For the downward refracting environment (see table 5.1), the spread in TL increases with range and the skewness is much larger at ranges of 10000 and 20000 m. Positive skewness values correspond to a long right tail in the probability distribution of TL. For the isovelocity environment (see table 5.2), the spread does not significantly increase with range and the skewness is small at ranges of 10000 and 20000 yd.

range (yd)	*mean TL (dB)*	*std dev TL (dB)*	*skewness TL*
1000	54.8	1.02	0.489
3000	63.7	1.65	0.443
10000	76.6	2.97	0.642
20000	87.0	4.69	0.811

Table 5.1. Statistical properties of transmission loss at ranges of 1000, 3000, 10000 and 20000 yd in a downward-refracting waveguide. Bottom loss is represented via an extreme value distribution with parameters α = 3 dB and β = 1 dB.

range (yd)	*mean TL (dB)*	*std dev TL (dB)*	*skewness TL*
1000	54.5	0.924	0.394
3000	62.8	1.27	0.168
10000	72.7	1.40	–0.045
20000	78.5	1.35	–0.137

Table 5.2. Statistical properties of transmission loss at ranges of 1000, 3000, 10000 and 20000 yd in an isovelocity waveguide. Bottom loss is represented via an extreme value distribution with parameters α = 3 dB and β = 1 dB.

We will now consider propagation in an upward refracting waveguide in which soundspeed linearly increases from the surface to the bottom. Two types of sound paths (or rays) are possible. At shallow grazing angles, sound will propagate via refracted surface reflected (RSR) rays that do not bounce off the ocean bottom. At steeper grazing angles, sound will propagate via bottom bounce (BB) rays. Apart from diffraction effects, RSR rays emanating from the source that have turning depths shallower than the depth of the receiver will not couple well to the receiver. In this case, the range-averaged, squared acoustic pressure at horizontal distance *r* from the source can be written as the sum of two terms:

$$\langle \mid p \mid^2 \rangle = \frac{4}{r} \int_{\chi_a}^{\chi_b} \exp(-\beta r) \frac{\cos(\chi_1)}{D(\chi_1)\sin(\chi)} d\chi_1 + \frac{4}{r} \int_{\chi_b}^{\pi/2} \mid V(\chi_h) \mid^{2N} \exp(-\beta r) \frac{\cos(\chi_1)}{D(\chi_1)\sin(\chi)} d\chi_1,$$

where (χ_a, χ_b) is the range of launch angles from the source that reach the depth of the receiver but do not strike the ocean bottom. The first integral represents propagation via the non-bottom interacting RSR ray paths and the second integral represents propagation via the bottom interacting BB paths.

Computations of transmission loss in an upward refracting waveguide with surface soundspeed 1500 m/s and bottom sound speed of 1520 m/s are shown in figure 5.27. The acoustic source is assumed to be located near the surface. The water depth is 300 m and the receiver is located at the midpoint of the water column. Three levels of bottom loss are considered: 1.5 dB, 3 dB and 6 dB. The probability distribution of transmission loss at ranges of 1000 yd, 3000 yd and 10000 yd are shown in figure 5.28. Mean TL, standard deviation of TL and skewness of TL for the upward refracting waveguide are given in table 5.3. The model of bottom loss shown in figure 5.24 has been assumed to apply in figure 5.28 and table 5.3.

Referring to table 5.3, we see that standard deviation of transmission loss now decreases with range for ranges beyond 3000 yd and the skewness of the probability density of transmission loss becomes negative at longer ranges. We have, in effect, a reversal of conditions in comparison to the downward refracting environment. In the upward refracting environment, the RSR paths do not interact with the bottom and as a result, there is no transmission variability associated with these paths. At long ranges, where the BB paths are very weak, RSR propagation dominates and variability decreases. The negative skewness in the probability density of transmission at longer ranges arises from the fact that smaller transmission loss values (less total loss) can only result from anomalously high BB path contributions.

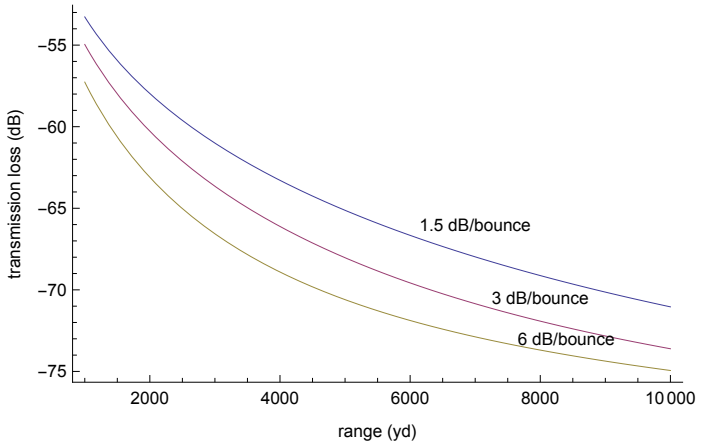

Figure 5.27. Range averaged transmission loss in an upward-refracting waveguide.

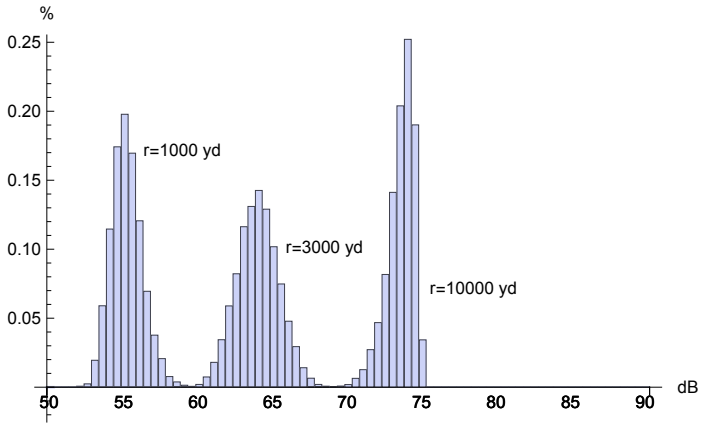

Figure 5.28. Probability distribution of transmission loss in an upward refracting waveguide.

range (yd)	*mean TL (dB)*	*std dev TL (dB)*	*skewness TL*
1000	54.5	1.05	0.425
3000	64.2	1.41	0.035
10000	73.8	0.914	–1.08
20000	77.9	0.363	–2.50

Table 5.3. Statistical properties of transmission loss at ranges of 1000, 3000, 10000 and 20000 yd in an upward-refracting half channel waveguide. Bottom loss is represented via an extreme value distribution with parameters $\alpha = 3$ dB and $\beta = 1$ dB.

5.9 Computation of selected figures

Figure 5.1

In[ ]:=

Figure 5.1 is computed via the following:

In[ ]:=
```
Clear[SL, N0, T, zpfa0, snr, PD];
SL = 160.0; N0 = 80.0; T = 1; zpfa0 = 4.75342;
snr[r_] := T * 10^(SL-N0)/10 / Max[r^2, 1]
PD[r_, zpfa_] := CDF[NormalDistribution[0, 1], Sqrt[2 snr[r]] - zpfa]
Plot[PD[r, zpfa0], {r, 0, 10 000}, ...]
```

Out[ ]=

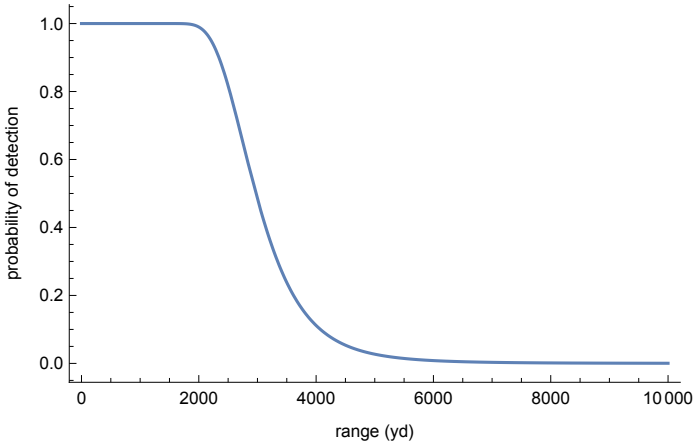

In[ ]:=

Figure 5.2

Figure 5.2 is computed via the following:

In[ ]:=
```
Clear[PdMatchedFilter, Pfa];
PdMatchedFilter[SNRdB_, Pfa_] := Block[{zpfa, x, snr},
  zpfa = x /. FindRoot[CDF[NormalDistribution[0, 1], x] == 1.0 - Pfa, {x, 4}] ;
  snr = 10^(SNRdB/10);
  1 - CDF[NormalDistribution[0, 1], zpfa - Sqrt[2 snr]]]
Pfa = 10^-6;
Plot[{PdMatchedFilter[SNRdB, Pfa]}, {SNRdB, 0, 25}, ...]
```

Out[ ]=

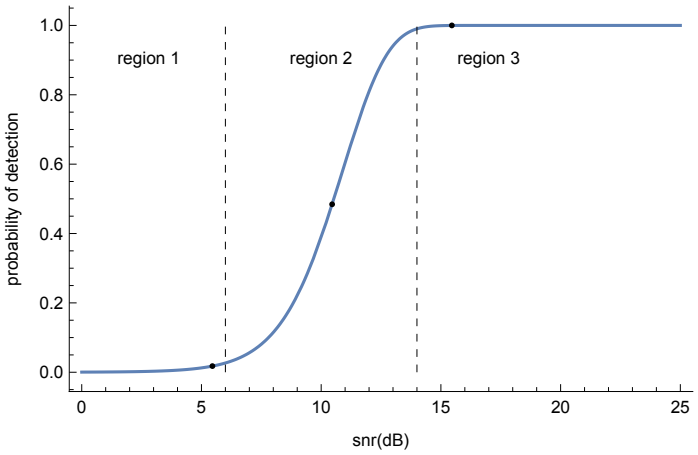

In[ ]:=

Figure 5.3

Figure 5.3 is computed via the following:

In[ ]:=
```
Clear[pTL, TLmode, σSpread, r1, r2];

pTL[x_, α_, β_] := e^(-e^((-x+α)/β) + (-x+α)/β) / β

TLmode[r_] := If[r < 1000, 20.0 Log[10, r], 60 + 10 Log[10, r / 1000]] + 0.0005 r

σSpread[r_] := 10 Log[10, r/1000 π^2/6]

r1 = 1000.0; r2 = 5000.0;

Plot[{pTL[x, TLmode[r1], σSpread[r1]],
  pTL[x, TLmode[r2], σSpread[r2]], pTL[x, 60 + 2.5, 5.57]}, {x, 40, 120}, ...]
```

Out[ ]=

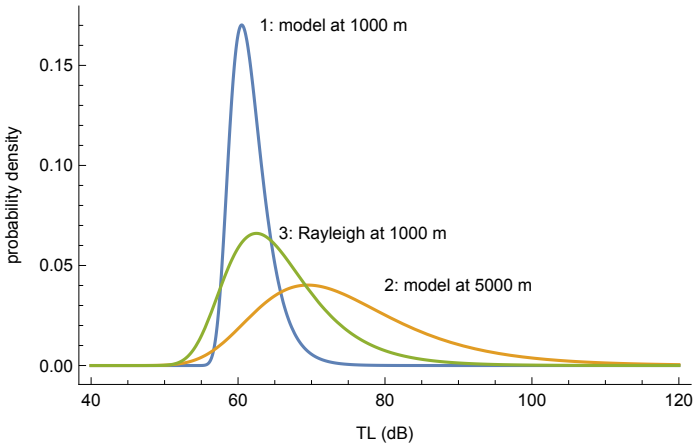

In[ ]:=

Figure 5.11

Figure 5.11 is computed via the following:

In[ ]:=
```
r1 = 1000.0;
r2 = 2000.0;
r3 = 5000.0;
r4 = 10 000.0;
SL = 160;
AN = 80;
Pfa = 10^-6;
PDnorm = pTL[TLmode[r1], TLmode[r1], σSpread[r1]]; ps = PDnorm;
Plot[{pTL[SL - AN - SNR, TLmode[r1], σSpread[r1]] / ps,
  pTL[SL - AN - SNR, TLmode[r2], σSpread[r2]] / ps,
  pTL[SL - AN - SNR, TLmode[r3], σSpread[r3]] / ps,
  pTL[SL - AN - SNR, TLmode[r4], σSpread[r4]] / ps,
  PdMatchedFilter[SNR, Pfa]}, {SNR, -20, 30}, ...]
```

Out[ ]=

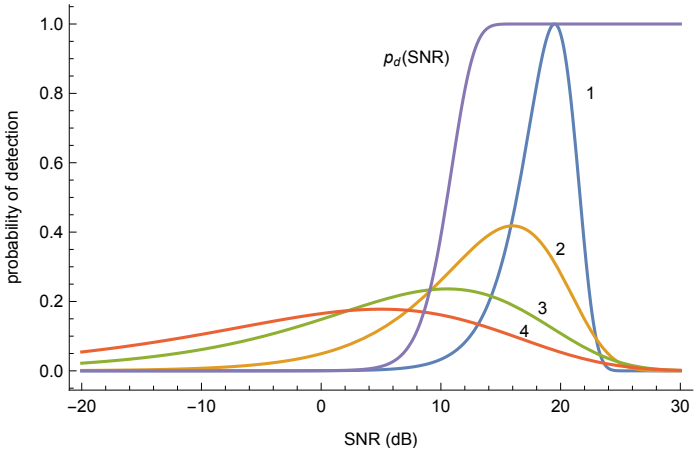

In[ ]:=

Figure 5.12

Figure 5.12 is computed via the following:

In[ ]:=
```
Clear[PdActive, SLact, TS1, TS2, ANact, Pfa];
PdActive[r_, SL_, TS_, AN_, Pfa_] := Module[{x, zpfa, r1, TL, SNRdB, snr},
  zpfa = x /. FindRoot[CDF[NormalDistribution[0, 1], x] == 1.0 - Pfa, {x, 4}];
  r1 = Max[r, 1]; TL = 20 Log[10, r1];
  SNRdB = SL - 2 TL + TS - AN;
  snr = 10^(SNRdB/10);
  1 - CDF[NormalDistribution[0, 1], zpfa - Sqrt[2 snr]]]
SLact = 220; TS1 = -5; TS2 = 10.0; ANact = 80; Pfa = 10^-6;
Plot[{PdActive[r, SLact, TS1, ANact, Pfa], PdActive[r, SLact, TS2, ANact, Pfa]},
 {r, 500, 5000}, ...]
```

Out[ ]=

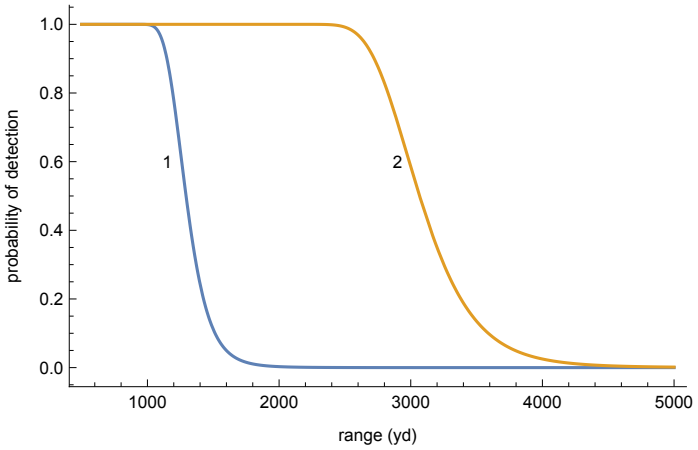

In[ ]:=

Figure 5.13

Figure 5.13 is computed via the following:

In[ ]:=
```
Clear[PH1, PH2, SLact, TS1, TS2, ANact, Pfa, ProbH1, ProbH2];
PH1[r_] := (PdActive[r, SLact, TS1, ANact, Pfa] ProbH1) /
    (PdActive[r, SLact, TS1, ANact, Pfa] ProbH1 +
      PdActive[r, SLact, TS2, ANact, Pfa] ProbH2);
PH2[r_] := 1 - PH1[r];
SLact = 220;
TS1 = -5;
TS2 = 10.0;
ANact = 80;
Pfa = 10^-6;
ProbH1 = 0.999;
ProbH2 = 1 - ProbH1;
SLact = 220;
TS1 = -5;
TS2 = 10.0;
ANact = 80;
Pfa = 10^-6;
ProbH1 = 0.999;
ProbH2 = 1 - ProbH1;
Plot[{PH1[r], PH2[r], PdActive[r, SLact, TS1, ANact, Pfa],
  PdActive[r, SLact, TS2, ANact, Pfa]}, {r, 500, 5000}, ...]
```

Out[ ]=

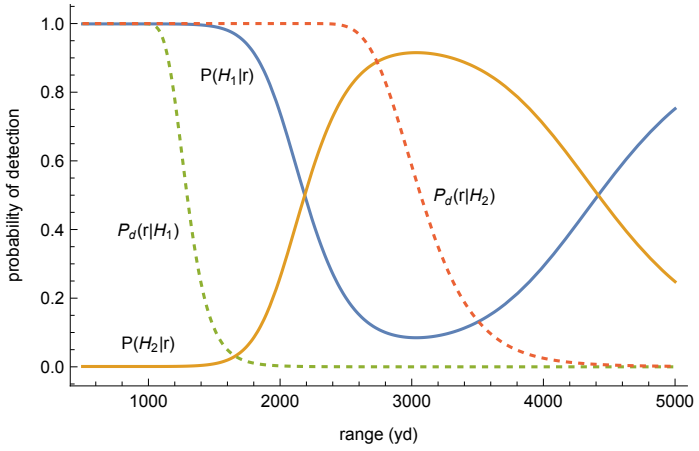

In[ ]:=

Figure 5.16

Figure 5.16 is computed via the following:

In[ ]:=
```
Clear[PdRayleighFade, PdMatchedFilter, Pfa];
PdRayleighFade[SNRdB_, Pfa_] := Block[{snr},
  snr = 10^(SNRdB/10);
  Pfa^(1/(1+snr))]
PdMatchedFilter[SNRdB_, Pfa_] := Block[{zpfa, x, snr},
  zpfa = x /. FindRoot[CDF[NormalDistribution[0, 1], x] == 1.0 - Pfa, {x, 4}] ;
  snr = 10^(SNRdB/10);
  1 - CDF[NormalDistribution[0, 1], zpfa - Sqrt[2 snr]]]
Pfa = 10^-6;
Plot[{PdMatchedFilter[SNRdB, Pfa], PdRayleighFade[SNRdB, Pfa]},
 {SNRdB, 0, 25}, ...]
```

Out[ ]=

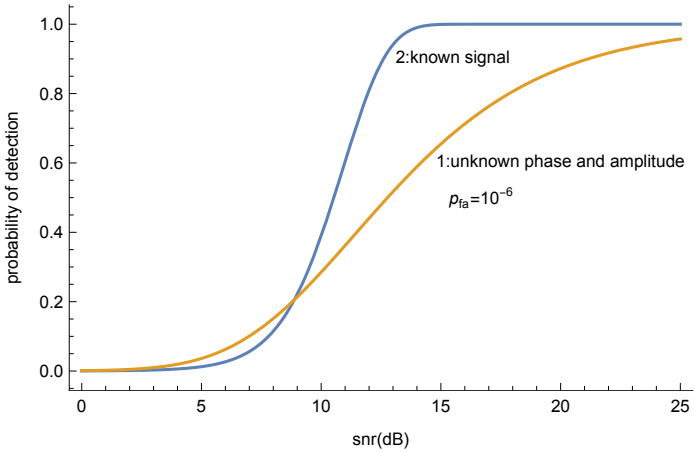

In[ ]:=

Figure 5.17

Figure 5.17 is computed via the following:

In[ ]:=
```
Clear[PD, v, vprime, f, g, Pfa, SNRdB1, SNRdB2, SNRdB3, SNRdB4, δdB];
PD[snr_, Pfa_] := Pfa^(1/(1+snr))
v[pd_, Pfa_] := Log[Pfa]/Log[pd] - 1
vprime[pd_, Pfa_] := -Log[Pfa]/(pd Log[pd]^2)
f[snr_, snr0_] := 1/(Sqrt[2] snr0 - snr0/Sqrt[2])
g[pd_, SNRdB_, δdB_, Pfa_] := Module[{ratio, snr0, snr1, snr2, pd1, pd2},
  snr0 = 10^(SNRdB/10); ratio = 10^(δdB/10); snr1 = snr0 / ratio; snr2 = ratio * snr0;
  pd1 = PD[snr1, Pfa]; pd2 = PD[snr2, Pfa];
  If[pd < pd1, 0, If[pd > pd2, 0, 1/(snr2 - snr1) vprime[pd, Pfa]]]]
Pfa = 10^-6; SNRdB1 = 3; SNRdB2 = 10; SNRdB3 = 17; SNRdB4 = 26; δdB = 1.5;
Plot[{g[pd, SNRdB1, δdB, Pfa], g[pd, SNRdB2, δdB, Pfa],
  g[pd, SNRdB3, δdB, Pfa], g[pd, SNRdB4, δdB, Pfa]}, {pd, 0, 1}, ...]
```

Out[ ]=

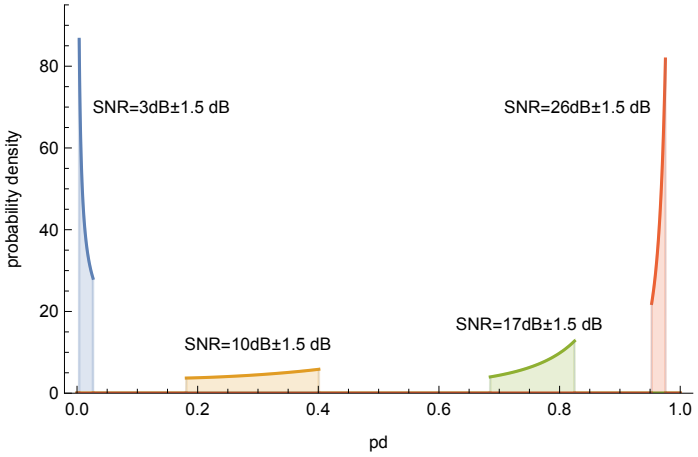

In[ ]:=

Figure 5.18

Figure 5.18 is computed via the following:

In[ ]:=
```
Pfa = 10^-6; SNRdB1 = 3; SNRdB2 = 10; SNRdB3 = 17; SNRdB4 = 26; δdB = 3;
Plot[{g[pd, SNRdB1, δdB, Pfa], g[pd, SNRdB2, δdB, Pfa],
  g[pd, SNRdB3, δdB, Pfa], g[pd, SNRdB4, δdB, Pfa]}, {pd, 0, 1}, ···]
```

Out[ ]=

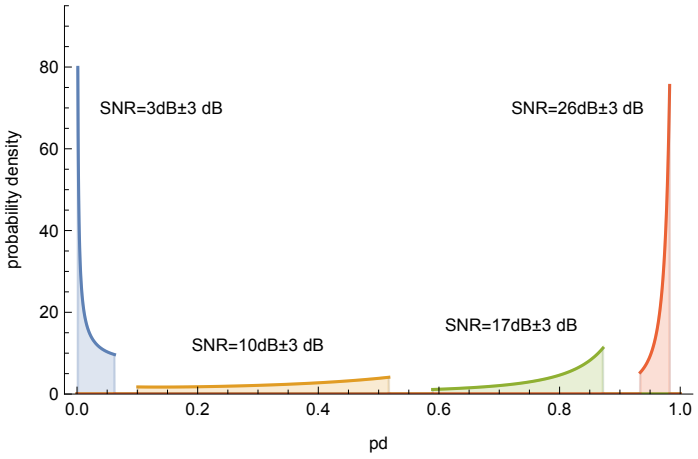

In[ ]:=

Figure 5.19

Figure 5.19 is computed via the following:

In[ ]:=
```
Pfa = 10^-6; SNRdB1 = 3; SNRdB2 = 10; SNRdB3 = 17; SNRdB4 = 26; δdB = 6;
Plot[{g[pd, SNRdB1, δdB, Pfa], g[pd, SNRdB2, δdB, Pfa],
  g[pd, SNRdB3, δdB, Pfa], g[pd, SNRdB4, δdB, Pfa]}, {pd, 0, 1}, ···]
```

Out[ ]=

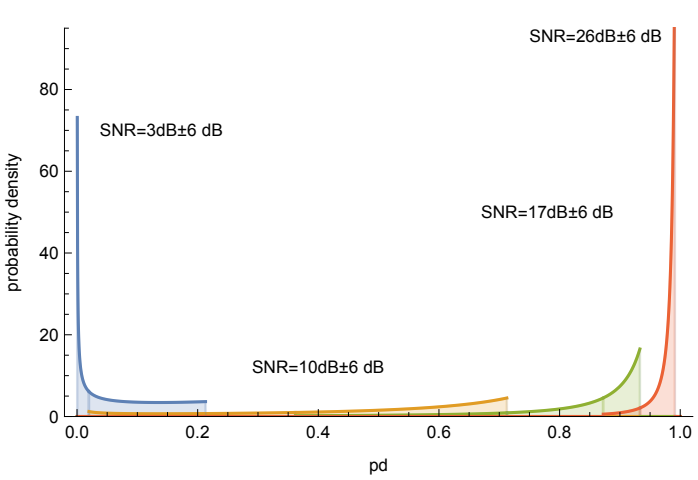

In[ ]:=

Figure 5.20

Figure 5.20 is computed via the following:

In[ ]:=
```
Clear[gEntropy, Pfa, δdB1, δdB2, δdB3];
gEntropy[SNRdB_, δdB_, Pfa_] :=
 Module[{snr0, ratio, snr1, snr2, pd1, pd2, Ns, dpd, pdd, q, pdtemp},
  snr0 = 10^(SNRdB/10.0); ratio = 10^(δdB/10.0); snr1 = snr0 / ratio; snr2 = ratio * snr0;
  pd1 = PD[snr1, Pfa]; pd2 = PD[snr2, Pfa];
  Ns = 101;
  dpd = (pd2 - pd1) / (Ns - 1);
  pdd = Table[pd1 + (q - 1) dpd, {q, 1, Ns}];
  -dpd * Sum[pdtemp = g[pdd[[q]], SNRdB, δdB, Pfa];
    pdtemp * Log[pdtemp], {q, 1, Ns}]
 ]
Pfa = 10^-6; δdB1 = 1.5; δdB2 = 3; δdB3 = 6;
Plot[{gEntropy[SNRdB, δdB1, Pfa], gEntropy[SNRdB, δdB2, Pfa],
  gEntropy[SNRdB, δdB3, Pfa]}, {SNRdB, 0, 25}, ...]
```

Out[ ]=

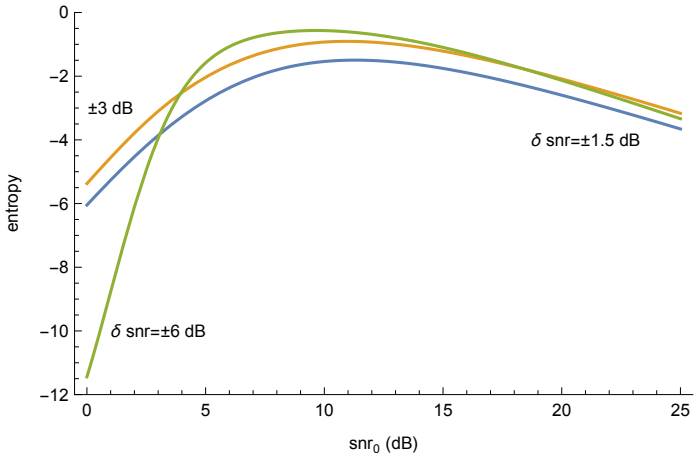

References

Blake, Lamont V. (1991), *Radar Range-Performance Analysis*, Munro Publishing Co.

Brekhovskikh, L. and Lysanov, Yu. (1982), *Fundamentals of Ocean Acoustics*, Springer Verlag.

Burdic, William S. (1984), *Underwater Acoustic System Analysis*, Prentice-Hall.

Elmore, W.C. and Heald, A.H. (1969), *Physics of Waves*, Dover Publications.

Gregory, Phil (2005), *Bayesian Logical Data Analysis for the Physical Sciences,* Cam ridge University Press.

Hammersley, J.M. and Handscomb, D.C. (1964), *Monte Carlo Methods*, Chapman and Hall.

Hogg, R.V. and Tanis, E.A. (2006), *Probability and Statistical Inference*, Pearson Prentice Hall, 7th edition.

Hudson, J.A. (1980), *The Excitation and Propagation of Elastic Waves*, Cambridge University Press.

Jaynes, E.T. (2003), *Probability Theory: The Logic of Science*, edited by G. Larry Bretthorst, Cambridge

University Press, reprinted 2009.

Jeffreys, Harold, (1973), *Scientific Inference*, Cambridge University Press, 3rd edition.

Jeffreys, Harold, (1976), *The Earth: Its Origin, History and Physical Constitution*, Cambridge University Press, 6th edition.

Jensen, F.B., Kuperman, W.A., Porter, M.B. and Schmidt, H. (1994), *Computational Ocean Acoustics*, American Institute of Physics.

Kimall, G.E. and Morse, P. M. (1970), *Methods of Operations Research*, Peninsula Publishing.

Koopman, Bernard O. (1980), *Search and Screening*, Pergamon Press, republished by The Military Operations Research Society 1999.

Officer, C.B. (1958), *Introduction to the Theory of Sound Transmission*, McGraw-Hill Book Company.

Ol'shevskii, V.V. (1978), *Statistical Methods in Sonar*, technical editor David Middleton, Studies in Soviet Science, Consultants Bureau.

Rees, W.G. (2001), *Physical Principles of Remote Sensing*, Cambridge University Press, 2nd edition.

Ross, Sheldon M. (1972), *Introduction to Probability Models*, Academic Press.

Selin, Ivan. (1965), *Detection Theory*, Princeton University Press.

Skudrzyk, E. (1971), *The Foundations of Acoustics*, Springer-Verlag.

Tucker, D.G. and Gazey, B.K. (1977), *Applied Underwater Acoustics*, Pergamon Press.

Urick, Robert J. (1983), *Principles of Underwater Sound*, McGraw-Hill Book Company.

Whalen, Anthony D. (1971), *Detection of Signals in Noise*, Academic Press.